

A Family of Mixed-Metal Cyanide Cubes with Alternating Octahedral and Tetrahedral Corners Exhibiting a Variety of Magnetic Behaviors Including Single Molecule Magnetism

Eric J. Schelter,[§] Ferdi Karadas,[†] Carolina Avendano,[†] Andrey V. Prosvirin,[†]
Wolfgang Wernsdorfer,[‡] and Kim R. Dunbar^{*,†}

Contribution from the Department of Chemistry, Texas A&M University, P.O. Box 30012,
College Station, Texas 77842-3012, Institute Néel, CNRS, BP 166, 25 Avenue des Martyrs,
38042 Grenoble Cedex 9, France

Received November 30, 2006; E-mail: dunbar@mail.chem.tamu.edu

Abstract: A series of structurally related pseudocubic metal cyanide clusters of Re(II) and 3d metal ions $[\{MX\}_4\{Re(triphos)(CN)_3\}_4]$ ($M = Mn, Fe, Co, Ni, Zn$; $X = Cl, I, -OCH_3$) have been prepared, and their magnetic and electrochemical properties have been probed to evaluate the effect of changing the identity of the 3d metal ion. Electrochemistry of the clusters reveals several rhenium-based oxidation and reduction processes, some of which result in cluster fragmentation. The richest electrochemistry was observed for the iron congener, which exists as the Re(I)/Fe(III) cluster at the resting potential and exhibits six clear one-electron reversible redox couples and two, closely spaced one-electron quasi-reversible processes. The $[\{Mn^{II}Cl\}_4\{Re^{II}(triphos)(CN)_3\}_4]$ complex exhibits single molecule magnetism with a fast tunneling relaxation process observed at $H = 0$ determined by micro-SQUID magnetization measurements. A comparative evaluation of the magnetic properties across the series reveals that the compounds exhibit antiferromagnetic coupling between the metal ions, except for $[\{Ni^{II}Cl\}_4\{Re^{II}(triphos)(CN)_3\}_4]$ that shows ferromagnetic behavior. Despite the large ground-state spin value of $[\{Ni^{II}Cl\}_4\{Re^{II}(triphos)(CN)_3\}_4]$ ($S = 6$), only manganese congeners exhibit SMM behavior to 1.8 K.

Introduction

Since the initial report of slow paramagnetic relaxation in isolated molecules dubbed single molecule magnetism (SMM),¹ numerous complexes have been observed to exhibit this effect. The first example and most studied SMM is a compound from the Mn_{12} oxide family of clusters, namely $[Mn_{12}O_{12}(O_2CCH_3)_{16}(H_2O)_4]$.² The magnetic properties of this molecule revealed that certain magnetically bistable molecules can exhibit seemingly macroscopic magnetic phenomena such as magnetic hysteresis by virtue of a combination of a large spin ground state and magnetic anisotropy in the form of a negative axial zero field splitting. SMMs are also attracting interest due to observation of quantum tunneling of their magnetization.^{3,4} Although substitution of the periphery ligands in $[Mn_{12}O_{12}(O_2CR)_{16}(H_2O)_4]$ has been shown to be quite facile^{5,6} and the development

of larger clusters has been furthered through reductive aggregation chemistry,⁷ selective chemical substitution of the core metal ions in these types of clusters has, as yet, not been reported.

Recently our group and others have shown the utility of metal cyanide chemistry in the preparation of high-spin clusters,^{8–15} several of which exhibit SMM behavior (Table 1). As amply demonstrated in the oxide chemistry, these studies have revealed the importance of inherent magnetic anisotropy of the individual ions that comprise the clusters for the observation of SMM behavior,^{8,9,14,16–19} a critical observation for the rational preparation of new molecules that behave in this manner. One source

[†] Texas A&M University.

[‡] Institute Néel, CNRS.

[§] Current address: MS J514 - Los Alamos National Laboratory, Los Alamos, NM 87545.

- (1) Sessoli, R.; Gatteschi, D.; Caneschi, A.; Novak, M. A. *Nature* **1993**, *365*, 141.
- (2) Eppley, H. J.; Tsai, H.-L.; de Vries, N.; Folting, K.; Christou, G.; Hendrickson, D. N. *J. Am. Chem. Soc.* **1995**, *117*, 301.
- (3) Thomas, L.; Lioni, F.; Ballou, R.; Gatteschi, D.; Sessoli, R.; Barbara, B. *Nature* **1996**, *383*, 145.
- (4) Gatteschi, D.; Sessoli, R. *Angew. Chem., Int. Ed.* **2003**, *42*, 268.
- (5) Ruiz-Molina, D.; Gerbier, P.; Rumberger, E.; Amabilino, D. B.; Guzei, I. A.; Folting, K.; Huffman, J. C.; Rheingold, A.; Christou, G.; Veciana, J.; Hendrickson, D. N. *J. Mater. Chem.* **2002**, *12*, 1152.
- (6) Zhao, H.; Berlinguette, C. P.; Bacsá, J.; Prosvirin, A. V.; Bera, J. K.; Tichy, S. E.; Schelter, E. J.; Dunbar, K. R. *Inorg. Chem.* **2004**, *43*, 1359.

- (7) Tasiopoulos, A. J.; Wernsdorfer, W.; Abboud, K. A.; Christou, G. *Angew. Chem., Int. Ed.* **2004**, *43*, 6338.
- (8) Rebilly, J.-N.; Mallah, T. *Struct. Bonding* **2006**, *122*, 103.
- (9) Long, J. R. In *Chemistry of Nanostructured Materials*; Yang, P., Ed.; World Scientific Publishing Co. Pte. Ltd.: Singapore, 2003; p 291.
- (10) Marvaud, V.; Decroix, C.; Scullier, A.; Tuyeras, F.; Guyard-Duhayon, C.; Vaissermann, J.; Marrot, J.; Gonnet, F.; Verdager, M. *Chem.-Eur. J.* **2003**, *9*, 1692.
- (11) Dunbar, K. R.; Heintz, R. A. *Prog. Inorg. Chem.* **1997**, *45*, 283–391.
- (12) Karadas, F.; Schelter, E. J.; Prosvirin, A. V.; Bacsá, J.; Dunbar, K. R. *Chem. Commun.* **2005**, 1414.
- (13) Li, D.; Parkin, S.; Wang, G.; Yee, G. T.; Prosvirin, A. V.; Holmes, S. M. *Inorg. Chem.* **2005**, *44*, 4903.
- (14) Song, Y.; Zhang, P.; Ren, X.-M.; Shen, X.-F.; Li, Y.-Z.; You, X.-Z. *J. Am. Chem. Soc.* **2005**, *127*, 3708.
- (15) Li, D.; Parkin, S.; Wang, G.; Yee, G. T.; Clerac, R.; Wernsdorfer, W.; Holmes, S. M. *J. Am. Chem. Soc.* **2006**, *128*, 4214.
- (16) Sokol, J. J.; Hee, A. G.; Long, J. R. *J. Am. Chem. Soc.* **2002**, *124*, 7656.
- (17) Choi, H. J.; Sokol, J. J.; Long, J. R. *Inorg. Chem.* **2004**, *43*, 1606.
- (18) Schelter, E. J.; Prosvirin, A. V.; Dunbar, K. R. *J. Am. Chem. Soc.* **2004**, *126*, 15004.
- (19) Berlinguette, C. P.; Vaughn, D.; Canada-Vilalta, C.; Galan-Mascaros, J. R.; Dunbar, K. R. *Angew. Chem., Int. Ed.* **2003**, *42*, 1523.

Table 1. Cyanide Clusters Exhibiting Slow Paramagnetic Relaxation with Data for Mn₁₂-acetate Shown for Comparison

compd	<i>S</i>	<i>D</i> (cm ⁻¹) ^a	<i>U</i> _{calc} ^b (cm ⁻¹)	<i>U</i> _{eff} ^c (cm ⁻¹)	<i>J</i> ^d (cm ⁻¹)	<i>τ</i> ₀ (s)	ref
Mn ₁₂ O ₁₂ (O ₂ CCH ₃) ₁₆ (H ₂ O) ₄	10	-0.46	46	43	-74.5 -29.5 -29.5 -22	2.1 × 10 ⁻⁷	1, 21, 22
K[(5-Brsalen) ₂ (H ₂ O) ₂ Mn ₂ Fe(CN) ₆]	7/2	<i>e</i>	<i>e</i>	25	+2.3	5.5 × 10 ⁻¹⁰	17
[{Mn ^{III} (C ₁₉ H ₂₀ N ₂ O ₂) ₂ } ₂ {W(bpy)(CN) ₆ }] ₂	5	-0.90	23	22	+0.83 +0.95	5.1 × 10 ⁻¹²	23
[Co ^{II} ₉ {W ^V (CN) ₈ } ₆ ·(CH ₃ OH) ₂₄]	21/2	<i>f</i>	<i>f</i>	19.32	<i>f</i>	7.39 × 10 ⁻¹¹	14
[Tp ₂ (Me ₃ tacn) ₃ Cu ₃ Fe ₂ (CN) ₆](ClO ₄) ₄	7	-5.7	34	16	+8.5(1)	4.8 × 10 ⁻⁸	24
K[(5-Brsalen) ₂ (H ₂ O) ₂ Mn ₂ Cr(CN) ₆]	5/2	<i>e</i>	<i>e</i>	16	-6.3	6.1 × 10 ⁻⁸	17
K[(Me ₃ tacn) ₆ MnMo ₆ (CN) ₁₈](ClO ₄) ₃	13/2	-0.33	14	10	-6.7	7 × 10 ⁻⁷	16
[Et ₄ N][{Mn ^{III} (salmen)(MeOH) ₂ } ₂ {Fe ^{III} (CN) ₆ }]	9/2	-0.87	17.4	9.7	+3.6	2.5 × 10 ⁻⁷	25
[{Mn ^{II} Cl} ₄ {Re ^{II} (triphos)(CN) ₃ } ₄]	"8" ^g	-0.391	25	8.8	<i>f</i>	3.25 × 10 ⁻⁷	18
[{(pzTp)Fe ^{III} (CN) ₃ } ₂ {Ni ^{II} (bpy) ₂ }]	2	-3.6	14.4	8.3	+7.0(2)	4 × 10 ⁻⁷	26
[Cr ^{III} [(CN)Ni(tetren)] ₆]	1	<i>f</i>	<i>f</i>	3.98	<i>f</i>	1.1 × 10 ⁻¹¹	8
[Tp*Fe ^{III} (CN) ₃ Ni ^{II} (DMF) ₄] ₂ [OTf] ₂	3	-3.98	35.8	<i>h</i>	+5.3	7 × 10 ⁻⁷	13
[Tp*Fe ^{III} (CN) ₃ Co ^{II} (DMF) ₄] ₂ [OTf] ₂	2	-3.04	12.2	<i>h</i>	-10	<i>h</i>	13
[{Mn ^{II} (tmphen) ₂ } ₃ {Mn ^{III} (CN) ₆ } ₂]	11/2	-0.348(3)	10	<i>h</i>	<i>f</i>	<i>h</i>	19
[{(pzTp)Fe ^{III} (CN) ₃ } ₄ {Ni ^{II} L} ₄][OTf] ₄	6	-0.23	8.3	<i>h</i>	+6.6	<i>h</i>	15
[Tp] ₈ (H ₂ O) ₆ Cu ^{II} ₆ Fe ^{III} ₈ (CN) ₂₄][ClO ₄] ₄	7	-0.16	7.8	<i>i</i>	+15	<i>h</i>	27
[Co ^{II} ₉ {Mo ^V (CN) ₈ } ₆ ·(CH ₃ OH) ₂₄]	21/2	<i>f</i>	<i>f</i>	<i>h</i>	<i>f</i>	<i>h</i>	14
[Co ^{II} ₉ {Re ^V (CN) ₈ } ₆ {Mo ^V (CN) ₈ } ₅ ·(CH ₃ OH) ₂₄]	20	<i>f</i>	<i>f</i>	<i>h</i>	<i>f</i>	<i>h</i>	28
[Co ^{II} ₉ {Re ^V (CN) ₈ } ₆ {W ^V (CN) ₈ } ₅ ·(CH ₃ OH) ₂₄]	20	<i>f</i>	<i>f</i>	<i>h</i>	<i>f</i>	<i>h</i>	28
[{Mn ^{III} (salen)(EtOH) ₃ } ₃ {Fe ^{III} (CN) ₆ }]	3/2	<i>e</i>	<i>e</i>	<i>h</i>	-2.8(1) +3.3(1)	<i>h</i>	29

^a Values obtained by fitting reduced magnetization data. ^b Predicted values calculated using *S* and *D*. *U*_{calc} = |*S*_z²*D*| for integer spin clusters and |(*S*_z² - 1/4)/*D*| for non-integer spin clusters. ^c Values obtained using Arrhenius plot. ^d Magnetic exchange Hamiltonian: *H* = -2*J*_{ij}*S*_i*S*_j. ^e Not reported due to presence of low-lying excited states. ^f Not reported. ^g The Re(II) ion in this cluster exhibits an orbital ²E ground state and, as such, cannot be described using a simple spin *S*. ^h While frequency-dependent signals were detected in χ'' using AC susceptometry, peaks were not detected in these signals to the low-temperature limit of the experiments. ⁱ An upper bound limit of 20 cm⁻¹ was determined using *τ*₀ = 10⁻¹⁰ s.

of magnetic anisotropy is ions that are known to possess a large, negative, axial zero-field splitting of their ground states. In the oxide chemistry this is accomplished by the presence of high-spin octahedral Mn(III) ions that exhibit an axial Jahn–Teller distortion.^{20–29} Studies by our group and others have shown that Mn(III) is also useful for the preparation of single molecule magnets from metal cyanide precursors.^{8,17,19,30,31}

Another source of magnetic anisotropy that can be exploited in the search for new SMMs is spin–orbit coupling.³² For example, the use of the Co(II) ion has led to the discovery of several oxide^{33,34} and octacyanometalate clusters that seem to indicate slow paramagnetic relaxation in recent years.^{14,23} While the large anisotropy of states of the Co(II) ion seem attractive, the magnitude of state separation afforded by spin–orbit coupling of this ion (*ζ* = 528 cm⁻¹) is small enough such that thermal population or admixture of excited states introduces barrier-tunneling direct relaxation processes that retard SMM

behavior. Therefore a logical synthetic strategy is to exploit ions with even larger spin–orbit coupling with the use of heavier transition metals such as those found in the 4d and 5d transition series. Examples of clusters based on 4d and 5d ions include the use of the octacyanometalate anions of Mo(V), W(V), and Re(V).²⁸ However, orbital quenching seems to play a detrimental role to reduce their inherent anisotropies. A particularly important result in this vein is the SMM behavior reported for the metal cyanide cluster [{Mo(Me₃tacn)(CN)₃}₆{Mn}]²⁺.¹⁶ It is imperative to note that when the analogous cluster is prepared using the Cr(III) ion instead of Mo(III) the cluster does not exhibit SMM behavior, which is attributed to the anisotropy of the Mo(III) ion vs the isotropic Cr(III) ion.¹⁶

As part of our research to identify suitable anisotropic 5d metal ion precursors for high-spin clusters, we recently undertook the synthesis and measured the magnetic properties of the d⁵ Re(II) complex: [Et₄N][Re^{II}(triphos)(CN)₃] (**1**) (triphos = 1,1,1-tris(diphenylphosphinoethyl)methane). The model that was developed to describe the magnetic data revealed an unusual temperature-independent paramagnetic behavior, owing to the trigonal distortion of the complex and a large spin–orbit coupling contribution (*ζ* = 2100 cm⁻¹) that yields a highly anisotropic orbital ²E magnetic ground state with a first excited ⁶A₁ state at 471 cm⁻¹ for **1**.^{35–37} We further reported the use of the [Re(II)(triphos)(CN)₃]⁻ building block to prepare mixed octahedral/tetrahedral cyanide cube clusters with divalent metal chlorides of Fe, Co, and Mn the latter of which exhibits SMM behavior.^{18,38} In this report we further demonstrate the general nature of the chemistry [Re(II)(triphos)(CN)₃]⁻ in the prepara-

- (20) Gerritsen, H. J.; Sabisky, E. S. *Phys. Rev.* **1963**, *132*, 1507.
- (21) Mukhin, A. A.; Travkin, V. D.; Zvezdin, A. K.; Lebedev, S. P.; Caneschi, A.; Gatteschi, D. *Europhys. Lett.* **1998**, *44*, 778.
- (22) Raghu, C.; Rudra, I.; Sen, D.; Ramasesha, S. *Phys. Rev. B: Condens. Matter* **2001**, *64*, 64419.
- (23) Yoon, J. H.; Jeong, H. L.; Hyoung, C. K.; Hong, C. S. *Inorg. Chem.* **2006**, ASAP.
- (24) Wang, C.-F.; Zuo, J.-L.; Bartlett, B. M.; Song, Y.; Long, J. R.; You, X.-Z. *J. Am. Chem. Soc.* **2006**, *128*, 7162.
- (25) Ferbinteanu, M.; Miyasaka, H.; Wernsdorfer, W.; Nakata, K.; Sugiura, K.; Yamashita, M.; Coulon, C.; Clerac, R. *J. Am. Chem. Soc.* **2005**, *127*, 3090.
- (26) Li, D.; Clerac, R.; Parkin, S.; Wang, G.; Yee, G. T.; Holmes, S. M. *Inorg. Chem.* **2006**, *45*, 5251.
- (27) Wang, S.; Zuo, J.-L.; Zhou, H.-C.; Choi, H. J.; Ke, Y.; Long, J. R.; You, X.-Z. *Angew. Chem., Int. Ed.* **2004**, *43*, 5940.
- (28) Freedman, D. E.; Bennett, M. V.; Long, J. R. *Dalton* **2006**, 2829.
- (29) Miyasaka, H.; Takahashi, H.; Madanbashi, T.; Sugiura, K.; Clerac, R.; Nojiri, H. *Inorg. Chem.* **2005**, *44*, 5969.
- (30) Choi, H. J.; Sokol, J. J.; Long, J. R. *J. Phys. Chem. Solids* **2004**, *65*, 839.
- (31) Beltran, L. M. C.; Long, J. R. *Acc. Chem. Res.* **2005**, *38*, 325.
- (32) Costes, J.-P.; Dahan, F.; Wernsdorfer, W. *Inorg. Chem.* **2006**, *45*, 5.
- (33) Yang, E.-C.; Hendrickson, D. N.; Wernsdorfer, W.; Nakano, M.; Zakharov, L. N.; Sommer, R. D.; Rheingold, A. L.; Ledezma-Gairaud, M.; Christou, G. *J. Appl. Phys.* **2002**, *91*, 7382.
- (34) Murrie, M.; Teat Simon, J.; Stoeckli-Evans, H.; Gudiel Hans, U. *Angew. Chem., Int. Ed.* **2003**, *42*, 4653.

- (35) Dunbar, K. R.; Schelter, E. J.; Tsukerblat, B. S.; Palii, A. V.; Ostrovsky, S. M.; Mirovitskii, V. Y.; Klokishner, S. I. *Adv. Quantum Chem.* **2003**, *44*, 413.
- (36) Dunbar, K. R.; Schelter, E. J.; Palii, A. V.; Ostrovsky, S. M.; Mirovitskii, V. Y.; Hudson, J. M.; Omary, M. A.; Klokishner, S. I.; Tsukerblat, B. S. *J. Phys. Chem. A* **2003**, *107*, 11102.
- (37) Dunbar, K. R.; Schelter, E. J.; Tsukerblat, B. S.; Ostrovsky, S. M.; Mirovitsky, V. Y.; Palii, A. V. *Polyhedron* **2003**, *22*, 2545.

tion of a family of isostructural pseudocubic clusters of Re(II) combined with metals spanning the 3d series from Mn to Zn. Of particular interest is the fact that, although the clusters belong to a homologous series, SMM behavior is observed in only one member of the family. Having a common structure available for a series of magnetic molecules and being able to systematically identify key parameters that affect magnetic properties is a valuable tool for future deliberate preparation of new SMMs.¹⁰

Experimental Section

Starting Materials. The starting material [Et₄N][Re(triphos)(CN)₃] (**1**) was prepared as reported, with a slight modification of the procedure. In the workup of the product, the volume of the reaction mixture was reduced in vacuo, and dry acetone (40 mL) was added to induce precipitation of the yellow product. The green supernatant was then removed, and the product was washed two additional times with minimal quantities of acetone. The product was recrystallized from acetonitrile/tetrahydrofuran to yield a bright-yellow, microcrystalline material. This method serves to increase the overall yield of the product and avoids contamination by the [Et₄N]Cl side product. Anhydrous metal chlorides M = Mn, Ni, Zn were purchased from the Strem Chemical Company and used without further purification. The tetrahydrofuran solvate clusters of Fe and Co, M₄Cl₈(THF)₆ were prepared as reported from the anhydrous metal chlorides (Strem).³⁹ Solvents were dried by conventional methods and distilled before use.

General Synthetic Methodology. The reaction of divalent metal chlorides with **1** leads to the formation of octanuclear clusters in high yields on time scales of minutes to hours. Polar organic solvents such as acetone and methanol ensure that the clusters precipitate as they form in most cases, although there is sufficient variability of the products' solubilities to warrant individual mention of the synthetic procedures employed (see Supporting Information).

The starting material **1** is oxidized slowly in the presence of moist air, and thus the introduction of water was scrupulously avoided during synthesis. In all cases, **1** and MCl₂ (M = Mn, Ni, Zn) or M₄Cl₈(THF)₆ (M = Fe, Co) were loaded in separate Schlenk flasks in a nitrogen atmosphere dry box. These flasks were then installed on a N₂ atmosphere Schlenk line and the addition reactions performed anaerobically. The clusters themselves are air-stable, allowing solid products to be handled, filtration-collected, and dried in air. The compounds reported show at least slight solubility in acetonitrile and are completely soluble in dichloromethane and tetrahydrofuran.

Synthesis of [MX]₄{Re(triphos)(CN)₃}₄ Clusters. [MnCl]₄{Re(triphos)(CN)₃}₄ (**2**): yield 0.122 g (0.031 mmol), 55%. Anal. Calc'd for **2**, C₁₇₆H₁₅₆N₁₂Cl₄P₁₂Fe₄Re₄: C, 53.96; H, 4.01; N, 4.29; Cl, 3.62. Found: C, 53.49; H, 4.05; N, 4.33; Cl, 3.35. IR(Nujol): ν = 2100, 2085 cm⁻¹ (C≡N); ES⁺-MS(CH₃CN/CH₂Cl₂, 1:1 mixture) m/z = 1939.16 ([M - Cl]²⁺), 1921.18 ([M - 2Cl]²⁺), 1268.80 ([M - 3Cl]³⁺). UV-vis(CH₂Cl₂): λ_{max} , nm (ϵ in M⁻¹ cm⁻¹) = 479 (6200).

[MnI]₄{Re(triphos)(CN)₃}₄ (**3**): yield 0.052 g (0.012 mmol), 14%. Anal. Calc'd for **3**, C₁₇₆H₁₅₆N₁₂I₄P₁₂Fe₄Re₄: C, 49.41; H, 3.83; N, 3.87. Found: C, 49.35; H, 3.67; N, 3.92. IR(Nujol): ν = 2096, 2081 cm⁻¹ (C≡N); ES⁺-MS(CH₃CN/CH₂Cl₂, 1:1 mixture) m/z = 2078 ([M - I]²⁺), 2014 ([M - 2I]²⁺), 1301 ([M - 3I]³⁺). UV-vis(CH₂Cl₂): λ_{max} , nm (ϵ in M⁻¹ cm⁻¹) = 481 (8500).

[FeCl]₄{Re(triphos)(CN)₃}₄ (**4**): yield: 0.053 g (63%). Anal. Calc'd for **4**, C₁₇₆H₁₅₆N₁₂Cl₄P₁₂Fe₄Re₄: C, 53.91; H, 4.01; N, 4.23; Cl, 3.62. Found: C, 53.52; H, 4.12; N, 4.19; Cl, 3.52. IR(Nujol): ν = 2011, 1992 cm⁻¹ (C≡N); Mössbauer (77.5 K): **1**: δ = 0.43 mm s⁻¹ (relative to RT Fe), ΔE = 0.53 mm s⁻¹. ES⁺-MS(CH₃CN/CH₂Cl₂, 1:1

mixture): m/z = 1960.10 ([M]²⁺). UV-vis(CH₂Cl₂): λ_{max} , nm (ϵ in M⁻¹ cm⁻¹) = 707 (67,000).

[FeCl]_{3.5}{Fe(OCH₃)(THF)_{0.5}Re(triphos)(CN)₃}₄ (**5**): yield 0.060 g (39%). Anal. Calc'd for **5**, C_{178.5}H₁₆₇N₁₂Cl_{3.5}OP₁₂Fe₄Re₄: C, 54.21; H, 4.12; N, 4.25; Cl, 3.14. Found: C, 53.27; H, 4.07; N, 4.30; Cl, 3.70. IR(Nujol): ν = 2010 and 1990 cm⁻¹ (C≡N). ES⁺-MS(CH₃CN/CH₂Cl₂, 1:1 mixture): m/z = 1943 ([M - CH₃O⁻ - C₂H₅O]²⁺), 1960 ([4]²⁺), and 1973 ([M - (C₂H₅O) + (CH₃O⁻)]²⁺). UV-vis(CH₂Cl₂): λ_{max} , nm (ϵ in M⁻¹ cm⁻¹) = 709 (58,000).

[CoCl]₄{Re(triphos)(CN)₃}₄ (**6**): yield 0.097 g (0.025 mmol), (65%). Anal. Calc'd for **6**, C₁₇₆H₁₅₆N₁₂Cl₄P₁₂Co₄Re₄: C, 53.74; H, 4.00; N, 4.27; Cl, 3.61. Found: C, 53.89; H, 4.16; N, 4.12; Cl, 3.58. IR(Nujol): ν = 2111, 2096 cm⁻¹ (C≡N). ES⁺-MS(CH₃CN/CH₂Cl₂, 1:1 mixture): m/z = 1966.19 ([M]²⁺), 1947.20 ([M - Cl]²⁺), 1930.20 ([M - 2Cl]²⁺). UV-vis(CH₂Cl₂): λ_{max} , nm (ϵ in M⁻¹ cm⁻¹) = 478.5 (7800), 614 (6400).

[NiCl]₄{Re(triphos)(CN)₃}₄ (**7**): yield 0.20 g (0.047 mmol), 74%. Anal. Calc'd for **7**, C₁₇₆H₁₅₆N₁₂Cl₄P₁₂Ni₄Re₄: C, 53.76; H, 4.00; N, 4.27; Cl, 3.61. Found: C, 53.39; H, 4.14; N, 4.46; Cl, 3.28. IR(Nujol): ν = 2122, 2109 cm⁻¹ (C≡N); ES⁺-MS(CH₃CN/CH₂Cl₂, 1:1 mixture): m/z = 1946.33 ([M - Cl]²⁺), 1930.30 ([M - 2Cl]²⁺), 1275.22 ([M - 3Cl]³⁺). UV-vis(CH₂Cl₂): λ_{max} , nm (ϵ in M⁻¹ cm⁻¹) = 401 (9700), 478 (8300).

[ZnCl]₄{Re(triphos)(CN)₃}₄ (**8**): yield 0.068 g (0.017 mmol), 27%. Anal. Calc'd for **8**, C₁₇₆H₁₅₆N₁₂Cl₄P₁₂Re₄Zn₄: C, 53.39; H, 3.97; N, 4.25. Found: C, 53.06; H, 4.11; N, 4.32. IR(Nujol): ν = 2127, 2115, 2102, 2074 cm⁻¹ (C≡N). ESI-MS(CH₃CN/CH₂Cl₂, 1:1 mixture) m/z = 1943.19 ([M - 2Cl]²⁺), 1952.19 ([M - 2Cl + H₂O]²⁺), 1961.00 ([M - 2Cl + 2H₂O]²⁺), 1923.24 ([M - 3Cl]²⁺), 1931.72 ([M - 3Cl + H₂O]²⁺), 1894.24 ([M - 4Cl - CN]²⁺), 1903.00 ([M - 4Cl - CN + H₂O]²⁺), 1912.00 ([M - 4Cl - CN + 2H₂O]²⁺). UV-vis(CH₂Cl₂): λ_{max} , nm (ϵ in M⁻¹ cm⁻¹) = 477 (6000).

Physical Measurements. Elemental analyses were performed by Atlantic Microlab, Inc. Infrared spectra were recorded as Nujol mulls between KBr plates with a Nicolet Nexus 470 FT-IR spectrometer. Electrospray mass spectra were collected at the Laboratory for Biological Mass Spectrometry at Texas A&M University using a PE Sciex (Concord, Ontario, Canada) API Qstar Pulsar with an Ionworks time-to-digital converter, TDCx4, for data recording. Samples dissolved in mixtures of dichloromethane and acetonitrile were electrosprayed and the data acquired in the positive-ion mode. Solution UV-visible absorption spectra were acquired using a Shimadzu UV-1601PC spectrophotometer. Electrochemical data were collected using a CH Instruments analyzer in dry dichloromethane or tetrahydrofuran containing 0.2 M tetra-*n*-butylammonium hexafluorophosphate as the supporting electrolyte. The working electrode was a BAS Pt disk electrode, the reference electrode was Ag/AgCl, and the counter electrode was a Pt wire. The Fc/Fc⁺ couple occurs at +0.48 V vs Ag/AgCl under the same experimental conditions. Magnetic measurements were performed on crushed microcrystalline samples with the use of a Quantum Design MPMS-XL SQUID magnetometer. DC magnetic susceptibility measurements were performed in the range of 1.8–300 K with an applied field of 0.1 T. AC magnetic susceptibility measurements were performed with a 3 Oe AC driving field in an operating frequency range of 1–1000 Hz. Magnetization data were collected in the 0–7 T range starting at zero field at 1.8 K. The data were corrected for the diamagnetic contributions calculated from the Pascal constants.⁴⁰ Micro-SQUID measurements were collected on samples of aligned single crystals at the temperatures indicated.

Results and Discussion

Synthesis of Molecular Cubes. The reaction of the d⁵ Re(II) containing salt [Et₄N][Re(triphos)(CN)₃] (**1**) with the

(38) Schelter, E. J.; Prosvirin, A. V.; Reiff, W. M.; Dunbar, K. R. *Angew. Chem., Int. Ed.* **2004**, *43*, 4912.

(39) Zhao, H.; Clerac, R.; Sun, J. S.; Ouyang, X.; Clemente-Juan, J. M.; Gomez-Garcia, C. J.; Coronado, E.; Dunbar, K. R. *J. Solid State Chem.* **2001**, *159*, 281.

(40) Mulay, L. N.; Boudreaux, E. A. *Theory and Applications of Molecular Diamagnetism*; Wiley: New York, 1976.

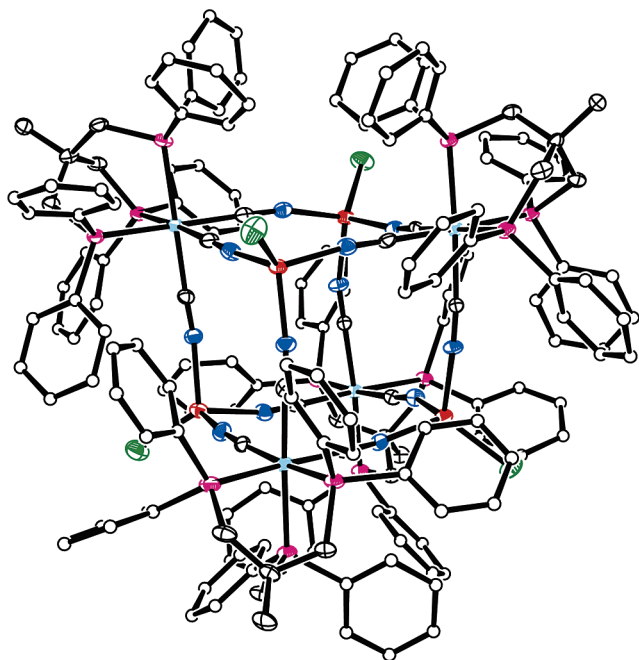


Figure 1. Thermal ellipsoid plot of $[\{\text{MnCl}\}_4\{\text{Re}(\text{triphos})(\text{CN})_3\}_4]$ (**2**) with ellipsoids projected at the 25% probability level. Phenyl carbons shown as spheres of arbitrary radius, and hydrogen atoms omitted for clarity. Color-coding: Re, light blue; Mn, red; C, white; N, dark blue; Cl, green; P, purple.

divalent metal starting materials MnCl_2 , MnI_2 , $\text{Fe}_4\text{Cl}_8(\text{THF})_6$, CoCl_2 , NiCl_2 , and ZnCl_2 yields the octanuclear metal cyanide clusters **2–8** with an approximate cubic geometry. Bulk reactions for the preparation of the clusters were performed in a slight excess of the $\text{Re}(\text{II})$ starting material to avoid contamination with byproducts of the paramagnetic 3d starting materials, several of which are susceptible to oxidation. The yields of the products vary depending on slight differences in the solubilities of the clusters. Mixtures of acetonitrile and acetone/acetonitrile, or acetone/methanol as the reaction media produced the highest yields for this general synthetic procedure. The introduction of methanol into the reaction solution used to prepare **4**, yielded an unexpected result. Under these conditions, a chloride is lost in favor of a THF and a methoxide ligand, but the substitution is incomplete, as evidenced by the elemental analytical data for **5**. Of the metals investigated, only the Re–Fe system was observed to undergo this transformation in the presence of methanol and THF.

Characterization of the Cube Clusters. Molecular Structures. Single-crystal X-ray diffraction experiments performed on **2**, **4–8** revealed that the products are distorted molecular “cubes” $[\{\text{MX}\}_4\{\text{Re}(\text{triphos})(\text{CN})_3\}_4]$ (Figure 1). Table 2 lists salient crystallographic parameters for the complexes while Table 3 lists important bond distances and angles for **2**. The cubes consist of four Re ions and four metal ions, M, where $\text{M} = \text{Mn}, \text{Fe}, \text{Co}, \text{Ni}, \text{Zn}$. The edges of the neutral clusters are spanned by 12 bridging cyanide ligands that link the metal ions. Charge neutrality is achieved by a balance of the charge of the metal cations with the negatively charged cyanide and chloride ligands (and in the case of **5**, one methoxide ligand). The ligand geometry around the $\text{Re}(\text{II})$ centers is similar to that of the mononuclear starting material, namely a distorted octahedron with the triphos ligands acting as a facially capping ligand with the carbon end of three cyanide ligands completing the coordination sphere. The 3d metal ions in the clusters adopt

four-coordinate distorted tetrahedral environments with three coordinated nitrogen atoms from bridging cyanide ligands and a fourth ligand extending out of the cube along a pseudo- C_3 -axis. The asymmetric unit in these studies consists of one entire cube and its accompanying solvent molecules.

The structures are approximate cubes in spite of the fact that four of the corners are distorted tetrahedra. The structures of **5**, **7**, and **8** exhibit N–M–N angles of $104.0(4)–119.1(6)^\circ$, $100.1(7)–108.3(7)^\circ$, $100.7(2)–104.6(3)^\circ$, respectively. As noted previously,^{18,38} observation of these large angles is counterintuitive to the geometric demands of a cubic structure. The fact that the structure forms and is quite stable attests to the remarkable flexibility of the cyanide ligand, indeed all of the C–Re–C values are less than 90° . None of the $\text{Re–C}\equiv\text{N}$ or $\text{C}\equiv\text{N–M}$ angles in **2** and **4–8** are strictly linear; they are reduced from 180° , allowing the edges of the cube to bend sufficiently to hold the framework together (Table 3). Examples of this type of distortion are found in a number of reported complex M–CN structures.^{41–44} Given the aforementioned structural features, the diagonal of each face of the cube connecting the Re ions is elongated, and the diagonal along each face of the cube connecting the 3d ions is compressed.

It is important to point out that the steric demand of the triphos ligands on the $\text{Re}(\text{II})$ centers enforces the distorted tetrahedral geometries at each of the M sites. Only a few other examples of compounds have been reported in the literature based on this effect.^{45–47} The phenyl substituents of the triphos ligands completely envelop the cube in an organic sheath and fit tightly together with edge-to-face π – π interactions.³⁸ The encapsulation of the metal centers by the envelope of organic substituents undoubtedly plays a role in the air- and moisture stability of the complexes. Overall the structure of these molecules arises as a result of a combination of the steric bulk of the triphos ligands and the flexibility of the cyanide bridges spanning the metal ions.

$[\{\text{MnI}\}_4\{\text{Re}(\text{triphos})(\text{CN})_3\}_4]$ (**3**). Unit cell determination for **3** ($a = 68.24(1) \text{ \AA}$, $b = 18.987(4) \text{ \AA}$, $c = 33.195(7) \text{ \AA}$, $\beta = 105.963(4)^\circ$) and elemental analysis revealed **3** to be isomorphous to complex **2**.

$[\{\text{FeCl}\}_{3.5}\{\text{Fe}(\text{OCH}_3)(\text{THF})\}_{0.5}\{\text{Re}(\text{triphos})(\text{CN})_3\}_4]$ (**5**). Inspection of the structure of **5** reveals differences in the coordination geometry of one of the iron sites respective to the other three (Figure 2). The atom $\text{Fe}(1)$ is compressed toward the center of the cube as a result of reduction of the $\text{Fe}(1)–\text{N}\equiv\text{C}$ angles from linearity. Substitutional disorder of $\text{Cl}(1)$ has affected this site with an exchange of $\text{Cl}(1)$ with one molecule of tetrahydrofuran. A methoxide ligand coordinated to $\text{Fe}(1)$ is also located in the internal cavity of the cube. The overall result of this distortion is that one of the corners of the cube is flattened, which is similar to that observed in **2**¹⁸ and **6**³⁸ with added substitutional disorder at the $\text{Fe}(1)$ site. The methoxide group compensates for the loss of one negative charge from the structure so that the cluster remains neutral. Metrical

- (41) Contakes, S. M.; Rauchfuss, T. B. *Angew. Chem., Int. Ed.* **2000**, *39*, 1984.
- (42) Contakes, S. M.; Rauchfuss, T. B. *Chem. Commun.* **2001**, 553.
- (43) Falvello, L. R.; Garde, R.; Tomas, M. J. *Cluster Sci.* **2000**, *11*, 125.
- (44) Akitsu, T.; Einaga, Y. *Inorg. Chem.* **2006**, *45*, 9826–9833.
- (45) Connelly, N. G.; Hicks, O. M.; Lewis, G. R.; Orpen, A. G.; Wood, A. J. *Dalton* **2000**, 1637.
- (46) Jacob, V.; Mann, S.; Huttner, G.; Walter, O.; Zsolnai, L.; Kaifer, E.; Rutsch, P.; Kircher, P.; Bill, E. *Eur. J. Inorg. Chem.* **2001**, 2625–2640.
- (47) Fritz, M.; Rieger, D.; Baer, E.; Beck, G.; Fuchs, J.; Holzmann, G.; Fehlhämmer, W. P. *Inorg. Chim. Acta* **1992**, *198–200*, 513.

Table 2. Crystallographic Data for **2** and **4–8**

compd	2	4	5	6	7	8
formula	C _{191.25} H _{179.25} N ₁₈ Cl ₄ P ₁₂ Re ₄ Mn ₄	C ₁₈₉ H _{174.75} N _{18.50} Cl ₄ P ₁₂ Re ₄ Fe ₄	C ₁₉₇ H ₁₉₆ N _{19.75} O ₂ Cl ₃ P ₁₂ Re ₄ Fe ₄	C ₁₉₅ H _{184.75} N _{20.50} Cl ₄ P ₁₂ Re ₄ Co ₄	C _{190.50} H _{178.75} N _{19.25} Cl ₄ P ₁₂ Re ₄ Ni ₄	C _{200.45} H _{184.25} N ₁₉ O _{2.70} Cl ₄ P ₁₂ Re ₄ Zn ₄
FW	4235.78	4186.86	4318.43	4317.34	4230.86	4422.24
T, K	110(2)	110(2)	100(2)	110(2)	110(2)	100(2)
space group	C2/c	C2/c	C2/c	C2/c	C2/c	C2/c
Z	8	8	8	8	8	8
a, Å	66.959(13)	66.829(19)	67.243(13)	66.803(13)	67.154(13)	67.056(13)
b, Å	18.977(4)	18.811(5)	18.813(4)	18.839(4)	19.104(4)	18.895(4)
c, Å	32.682(7)	32.575(9)	32.616(7)	32.491(7)	32.685(7)	32.549(7)
β, deg	106.92(3)	106.957(8)	106.44(3)	106.62(3)	106.96(3)	106.68(3)
V, Å ³	39730(14)	39170(19)	39574(14)	39182(14)	40110(14)	39504(14)
d _{calc} , g/cm ³	1.416	1.420	1.450	1.464	1.401	1.487
R1(wR2)	0.0651(0.1765)	0.1258(0.2838)	0.0800(0.1972)	0.0648(0.1520)	0.1016(0.2574)	0.0482(0.1265)

parameters for the Re(1–4), Fe(2), Fe(3), and Fe(4) ions in **5** are essentially the same as those observed in **4**.

The geometry of Fe(1) is that of a distorted trigonal bipyramid. The Fe–O distance to the THF ligand of 2.105(19) Å is consistent with five-coordinate complexes of Fe(III).⁴⁰ The Fe–OCH₃ distance of 2.381(19) Å is long in the context of Fe(III)–methoxide bond lengths, which are typically in the range of ~1.7–2.0 Å. The observed bond length is thought to be the result of steric effects of the neighboring cyanide ligands which are bent toward the methoxide, thereby preventing it from binding more tightly to the metal center. The Fe(III) site is globally distorted toward the methoxide ligand, thereby inducing the C≡N–M angles to decrease to values of 152.2(16), 161.1(12), and 162.5(12)°, but steric repulsion of these same cyanide ligands forces the methoxide ligand away from the metal center, resulting in a longer Fe–OCH₃ bond. Evidence for the methoxide-bound species in samples **5** was also corroborated by ES⁺-MS data (vide infra), which exhibits signals corresponding to loss of methoxide (*m/z* = 1943), the divalent molecular ion (*m/z* = 1960), and coordination of a second methoxide to the molecular ion (*m/z* = 1970).

[{ZnCl}₄]{Re(triphos)(CN)₃}]₄ (**8**). The molecular structure of **8** also revealed a single metal site disorder. The metal ion Zn(1A) exhibits a Zn–Cl ligand pointed inward to the central cavity of the structure, refined to an occupancy factor of 20% (Figure 3). The C≡N–Zn(1A) angles at this site range between 125.4(6)–130.4(6)°, which is in sharp contrast to the “external” Zn sites in the molecule whose C≡N–Zn angles range from 165.0(6)–175.2(6)°. These C≡N–Zn(1A) angles are much more acute in comparison to the other angles in this molecule. Precedent for such C≡N–Zn angles is found in nitrile complexes of tetrahedral Zn(II) with reported values of 112°⁴⁸ and 130.0(13)°.⁴⁹ The Zn(1A)–N4 distance of 1.901(8) Å is short as compared to the other Zn–N distances in the cluster (1.954(6)–2.010(6) Å), a difference attributed to the disorder of the Zn(1A) site. The two other Zn(1A)–N distances are consistent with other Zn–N distances observed in the structure. An additional peak of electron density inside the cluster is attributed to a disordered chloride that is not bound to Zn(1A). This additional component of disorder to Cl(1A), which was not modeled, accounts for the anomalously high thermal parameters observed for Cl(1A); similar examples of disordered cations in

the cavities of molecular cubes have been reported.⁵⁰ Evidence for the disorder at the Zn(1) site is reflected in the instability of the cluster as revealed by ES⁺-MS data collected on samples of **8**, whose lability at the Zn sites leads to fragmentation by loss of cyanide groups. The disordered Zn(1A) component also gives rise to a second set of C≡N stretches in the infrared spectrum of **8** (vide infra).

The Zn–Cl distances in **8** range from 2.202(2)–2.242(4) Å which are consistent with reported values for Zn(II)–Cl-containing compounds. The local geometries of the Zn sites are considerably distorted from ideal tetrahedral, with central angles N–Zn–Cl ranging from 114.1(2)–116.8(2)° and N–Zn–N ranging from 100.7(2)–104.6(3)°. The Re–Zn body diagonals of the cube reveal that a compression of one of the pseudo-*C*₃ axes, as observed throughout the series of clusters, is also present in this compound. In this case, the axis of compression is defined along the pseudo-*C*₃ axes of Re(3) and Zn(3), whose Re–Zn distance is ~0.21 Å shorter than the average of the other three Re–Zn distances. The internal cavity of the molecule is occupied by one methanol molecule whose occupancy is 20%, and by the partially occupied chloride ligand Cl(1A), which is within ~0.3 angstroms of the centroid of the distorted cube defined by the eight external metal ions. Other distances and angles in the structure of **8** are consistent with expected values.

Infrared Spectroscopy. The signatures of C≡N stretching modes render infrared spectroscopy a useful tool for the characterization of compounds **2–8**. In considering the series one would anticipate that the *ν*(C≡N) frequencies would shift from the starting material (**1**) values (2060, 2070 cm^{−1})⁵¹ to higher energy across the periodic series from **2** to **8**. This is generally the case in the clusters (Figure 4) with the exception of **4**. As reported previously, **4** undergoes a redox reaction during formation that involves an electron transfer from the Fe(II) to the Re(II) metal centers, resulting in a ground-state Re(I)₄Fe(III)₄ configuration;³⁸ this oxidation-state change is manifested in the energies of the C≡N stretches. Further evidence for this transformation was found by noting structural changes at the Re coordination sites, the accessibility of the reversible Re(II)→Re(I) electrochemical reduction couple for the starting material, and Mössbauer spectroscopy.^{38,51}

The IR spectrum of [{ZnCl}₄]{Re(triphos)(CN)₃}]₄ (**8**) exhibits two C≡N stretches at 2102, and 2074 cm^{−1} in addition

(48) Isakov, I. V.; Zvonkova, Z. V. *Dokl. Akad. Nauk SSSR* **1962**, *145*, 801.

(49) Seneque, O.; Rager, M.-N.; Giorgi, M.; Reinaud, O. *J. Am. Chem. Soc.* **2000**, *122*, 6183.

(50) Klausmeyer, K. K.; Wilson, S. R.; Rauchfuss, T. B. *J. Am. Chem. Soc.* **1999**, *121*, 2705.

(51) Schelter, E. J.; Bera, J. K.; Bacsá, J.; Galan-Mascaros, J. R.; Dunbar, K. R. *Inorg. Chem.* **2003**, *42*, 4256.

Table 3. Selected Bond Distances and Angles for $[(\text{MnCl})_4\{\text{Re}(\text{triphos})(\text{CN})_3\}_4]^{2-}$

atoms	distance/Å	atoms	distance/Å	atoms	angle/deg	atoms	angle/deg	atoms	angle/deg
Re(1)–C(1)	2.033(12)	Mn(1)–N(4)	2.088(10)	P(3)–Re(1)–P(1)	86.17(10)	P(8)–Re(3)–P(7)	87.37(10)	N(10)–Mn(1)–N(4)	98.6(4)
Re(1)–C(2)	2.075(10)	Mn(1)–N(9)	2.093(9)	P(3)–Re(1)–P(2)	84.53(9)	P(8)–Re(3)–P(9)	85.95(10)	N(10)–Mn(1)–N(9)	102.6(4)
Re(1)–C(3)	2.064(11)	Mn(1)–N(10)	2.071(10)	P(1)–Re(1)–P(2)	88.33(9)	P(7)–Re(3)–P(9)	87.06(10)	N(2)–C(2)–Re(1)	171.6(8)
Re(1)–P(1)	2.421(3)	Mn(1)–Cl(1)	2.298(4)	C(1)–Re(1)–C(3)	85.1(4)	C(7)–Re(3)–C(9)	84.2(4)	N(2)–C(2)–Mn(3)	175.0(9)
Re(1)–P(2)	2.425(3)	Mn(2)–N(1)	2.070(10)	C(1)–Re(1)–C(2)	84.8(4)	C(7)–Re(3)–C(8)	83.6(4)	C(2)–C(3)–Re(1)	164.8(8)
Re(1)–P(3)	2.418(3)	Mn(2)–N(7)	2.048(10)	C(3)–Re(1)–C(2)	86.0(4)	C(9)–Re(3)–C(8)	87.3(4)	N(3)–C(3)–Re(1)	177.4(9)
Re(2)–C(4)	2.067(12)	Mn(2)–N(12)	2.062(9)	C(1)–Re(1)–P(3)	97.5(3)	C(7)–Re(3)–P(8)	92.7(3)	C(3)–N(3)–Mn(4)	166.2(9)
Re(2)–C(5)	2.066(11)	Mn(2)–Cl(2)	2.282(4)	C(3)–Re(1)–P(1)	177.3(3)	C(9)–Re(3)–P(8)	94.2(3)	N(4)–C(4)–Re(2)	177.2(10)
Re(2)–C(6)	2.065(10)	Mn(3)–N(2)	2.077(8)	C(2)–Re(1)–P(3)	93.5(3)	C(8)–Re(3)–P(8)	92.7(3)	C(4)–N(4)–Mn(1)	166.9(9)
Re(2)–P(4)	2.420(3)	Mn(3)–N(5)	2.082(9)	C(1)–Re(1)–P(1)	176.1(3)	C(7)–Re(3)–P(7)	175.9(3)	N(5)–C(5)–Re(2)	175.3(9)
Re(2)–P(5)	2.426(3)	Mn(3)–N(11)	2.062(9)	C(3)–Re(1)–P(1)	91.2(3)	C(7)–Re(3)–P(7)	176.4(3)	C(5)–N(5)–Mn(3)	161.8(8)
Re(2)–P(6)	2.426(3)	Mn(3)–Cl(3)	2.317(3)	C(2)–Re(1)–P(1)	96.3(3)	C(8)–Re(3)–P(7)	92.2(3)	N(6)–C(6)–Re(2)	176.3(9)
Re(3)–C(7)	2.035(13)	Mn(4)–N(3)	2.082(9)	C(1)–Re(1)–P(2)	90.7(3)	C(7)–Re(3)–P(9)	96.6(3)	C(6)–N(6)–Mn(4)	165.5(9)
Re(3)–C(8)	2.045(11)	Mn(4)–N(6)	2.059(8)	C(3)–Re(1)–P(2)	96.1(3)	C(9)–Re(3)–P(9)	179.2(3)	N(7)–C(7)–Re(3)	175.8(10)
Re(3)–C(9)	2.051(13)	Mn(4)–N(8)	2.056(11)	C(2)–Re(1)–P(2)	174.8(3)	C(8)–Re(3)–P(9)	92.6(3)	C(7)–N(7)–Mn(2)	172.6(10)
Re(3)–P(7)	2.402(3)	Mn(4)–Cl(4)	2.303(3)	P(4)–Re(2)–P(5)	85.92(10)	P(10)–Re(4)–P(11)	86.10(12)	N(8)–C(8)–Re(3)	177.8(10)
Re(3)–P(8)	2.401(3)	C(1)–N(1)	1.166(13)	P(4)–Re(2)–P(6)	87.74(9)	P(10)–Re(4)–P(12)	88.91(10)	C(8)–N(8)–Mn(4)	163.7(9)
Re(3)–P(9)	2.402(3)	C(2)–N(2)	1.151(11)	P(5)–Re(2)–P(6)	86.82(10)	P(11)–Re(4)–P(12)	85.91(10)	N(9)–C(9)–Re(3)	177.2(10)
Re(4)–C(10)	2.075(12)	C(3)–N(3)	1.155(12)	C(6)–Re(2)–C(5)	86.7(4)	C(11)–Re(4)–C(12)	86.2(4)	C(9)–N(9)–Mn(1)	169.8(9)
Re(4)–C(11)	2.048(12)	C(4)–N(4)	1.156(13)	C(6)–Re(2)–C(4)	86.1(4)	C(11)–Re(4)–C(10)	87.2(4)	N(10)–C(10)–Re(4)	176.4(10)
Re(4)–C(12)	2.066(12)	C(5)–N(5)	1.154(12)	C(5)–Re(2)–C(4)	86.6(4)	C(12)–Re(4)–C(10)	84.3(4)	C(10)–N(10)–Mn(1)	168.8(10)
Re(4)–P(10)	2.404(3)	C(6)–N(6)	1.168(12)	C(6)–Re(2)–P(4)	95.6(3)	C(11)–Re(4)–P(10)	93.5(3)	N(11)–C(11)–Re(4)	177.2(8)
Re(4)–P(11)	2.404(3)	C(7)–N(7)	1.169(14)	C(5)–Re(2)–P(4)	89.3(3)	C(12)–Re(4)–P(10)	90.6(3)	C(11)–N(11)–Mn(3)	164.0(9)
Re(4)–P(12)	2.405(3)	C(8)–N(8)	1.166(13)	C(4)–Re(2)–P(4)	175.5(3)	C(10)–Re(4)–P(10)	174.8(3)	N(12)–C(12)–Re(4)	174.4(10)
		C(9)–N(9)	1.153(12)	C(6)–Re(2)–P(5)	90.9(3)	C(11)–Re(4)–P(11)	177.4(3)	C(12)–N(12)–Mn(2)	172.3(10)
		C(10)–N(10)	1.142(13)	C(5)–Re(2)–P(5)	174.5(3)	C(12)–Re(4)–P(11)	96.3(3)		
		C(11)–N(11)	1.174(12)	C(4)–Re(2)–P(5)	98.3(3)	C(10)–Re(4)–P(11)	93.5(3)		
		C(12)–N(12)	1.132(13)	C(6)–Re(2)–P(6)	175.9(3)	C(11)–Re(4)–P(12)	91.5(3)		
				C(5)–Re(2)–P(6)	95.8(3)	C(12)–Re(4)–P(12)	177.7(3)		
				C(4)–Re(2)–P(6)	90.8(3)	C(10)–Re(4)–P(12)	96.2(3)		

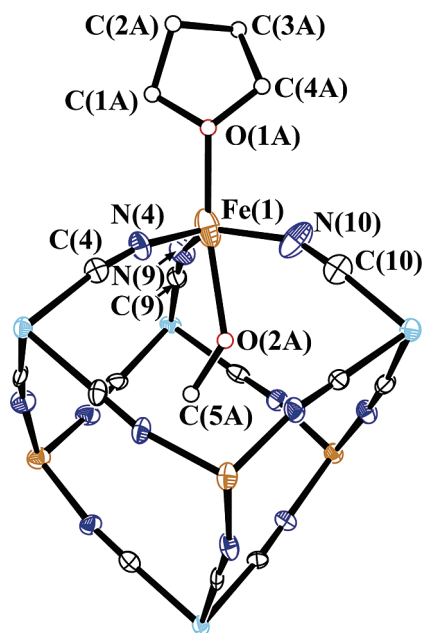


Figure 2. Partial molecular structure of $[\{\text{FeCl}\}_{3.5}\{\text{Fe}(\text{OCH}_3)(\text{THF})\}_{0.5}\{\text{Re}(\text{triphos})(\text{CN})_3\}_4]$ (**5**). Thermal ellipsoids projected at the 25% level. Triphos ligands, hydrogen, chlorine, and phosphorus atoms have been omitted for clarity. Disordered components (50% occupancy) shown as spheres of arbitrary radius. Color-coding: Re, light blue; Fe, gold; C, white; N, dark blue.

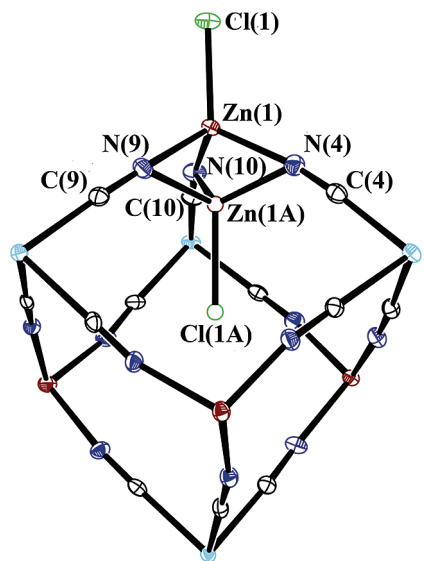


Figure 3. Partial molecular structure of $[\{\text{ZnCl}\}_4\{\text{Re}(\text{triphos})(\text{CN})_3\}_4]$ (**8**). Thermal ellipsoids projected at the 25% level. Triphos ligands, hydrogen, phosphorus, and three chlorine atoms have been omitted for clarity. Minor disordered components (15% occupancy) shown as spheres of arbitrary radius. Color-coding: Re, light blue; Zn, red; C, white; N, dark blue.

to the primary modes at 2127, 2115 cm^{-1} observed for the other members of the series. The additional two features are attributed to the disorder between the Zn(1) and Zn(1A) sites (*vide supra*). The $\text{C}\equiv\text{N}-\text{Zn}(1\text{A})$ angles of $125.4(6)-130.4(6)^\circ$ are sufficiently acute such that the energy of the $\text{C}\equiv\text{N}$ oscillator is not shifted to as high energies as the more linear $\text{C}\equiv\text{N}-\text{Zn}(1)$ modes; instead the vibration is at an intermediate value as compared to the starting material (2060, 2070 cm^{-1}).

Electrospray Mass Spectrometry. Electrospray mass spectrometry (ESI-MS) experiments performed in acetonitrile/dichloromethane using the soft ionization method of this

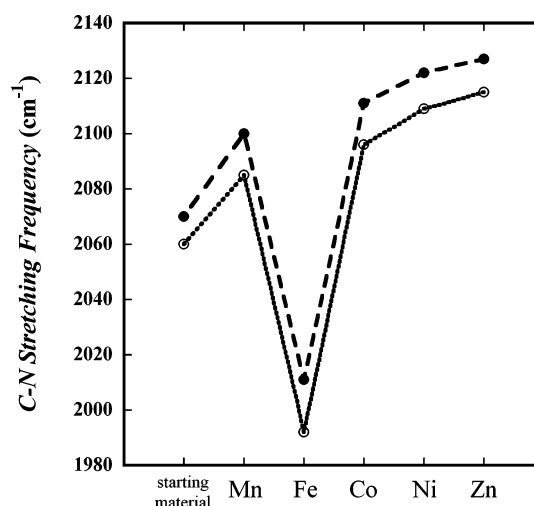


Figure 4. Primary IR stretching frequencies for compounds **1–2**, **4**, and **6–8** with lines shown as guides for the eye.

technique provided information on the solution stabilities of the clusters **2–8**.⁵² Positive-ion mode measurements revealed intact clusters in nearly all cases, with signals appearing for doubly charged species. In all cases except for **4**, fragmentation patterns occurred by loss of halide ligands (or methoxide in the case of **5**). The signal for **4** occurs at $m/z = 1960.10$ which corresponds to the doubly charged parent ion species: $[\{\text{FeCl}\}_4\{\text{Re}(\text{triphos})(\text{CN})_3\}_4]^{2+}$ with no loss of Cl^- ion, presumably due to the presence of the higher-charged Fe(III). In addition to the molecular ion peak for **4**, samples of **5** show two additional doubly charged signals at $m/z = 1943$ ($[\text{M} - \text{CH}_3\text{O}^- - \text{C}_2\text{H}_5\text{O}]^{2+}$) and 1973 ($[\text{M} - (\text{C}_2\text{H}_5\text{O}) + (\text{CH}_3\text{O}^-)]^{2+}$) where $\text{M} = [\{\text{FeCl}\}_3\{\text{Fe}(\text{OCH}_3)(\text{THF})\} - \{\text{Re}(\text{triphos})(\text{CN})_3\}_4]$, corresponding to the loss of the methoxide ligand from **5** and the coordination of **5** by a second methoxide ligand volatilized in the course of the experiment. Due to its lability, the bound THF solvent molecule in the structure of **5** was not observed in the mass spectrometry experiments.

The ESI-MS spectrum of $[\{\text{ZnCl}\}_4\{\text{Re}(\text{triphos})(\text{CN})_3\}_4]$ (**8**) contains a larger number of fragmentation products than any of the other compounds studied including species in which cyanide ligands have been lost; surprisingly, the core of the cluster is still intact. Several of the larger mass clusters also exhibit m/z values corresponding to the coordination of water, with structural core remaining intact.

Electrochemistry. Beginning with the body of work on Creutz–Taube type compounds,⁵³ and continuing through studies of multiple metal ion “grid” type complexes,^{54–57} electrochemical studies have indicated that strong electronic coupling is often observed across metal–metal cyanide bridges.^{58,59} Solution electrochemical studies performed on **2**,

- (52) Campos-Fernandez, C. S.; Schottel, B. L.; Chifotides, H. T.; Bera, J. K.; Bacsa, J.; Koomen, J. M.; Russell, D. H.; Dunbar, K. R. *J. Am. Chem. Soc.* **2005**, *127*, 12909.
- (53) Creutz, C. *Prog. Inorg. Chem.* **1983**, *30*, 1.
- (54) Hanan, G. S.; Volkmer, D.; Lehn, J.-M. *Can. J. Chem.* **2004**, *82*, 1428.
- (55) Ruben, M.; Rojo, J.; Romero-Salguero, F. J.; Uppadine, L. H.; Lehn, J.-M. *Angew. Chem., Int. Ed.* **2004**, *43*, 3644.
- (56) Uppadine, L. H.; Gisselbrecht, J.-P.; Kyritsakas, N.; Naettinen, K.; Rissanen, K.; Lehn, J.-M. *Chem.-Eur. J.* **2005**, *11*, 2549.
- (57) Milway, V. A.; Abedin, S. M. T.; Niel, V.; Kelly, T. L.; Dawe, L. N.; Dey, S. K.; Thompson, D. W.; Miller, D. O.; Alam, M. S.; Mueller, P.; Thompson, L. K. *Dalton* **2006**, 2835.
- (58) Oshio, H.; Onodera, H.; Tamada, O.; Mizutani, H.; Hikichi, T.; Ito, T. *Chem.-Eur. J.* **2000**, *6*, 2523.
- (59) Oshio, H.; Onodera, H.; Ito, T. *Chem.-Eur. J.* **2003**, *9*, 3946.

Table 4. Electrochemical Processes (DPV) Recorded for $[\{\text{MCl}\}_4\{\text{Re}(\text{triphos})(\text{CN})_3\}]$ Potentials Reported vs Ag/AgCl Reference Electrode

1	2	4	6	7	8
$E_{\text{ox}} (\text{V})$					
+1.12	+1.28	+1.42 ^c	+0.89	+1.20	+1.20
+0.19	+1.01	+1.26	+0.80	+0.98	+1.12 ^c
	+0.71	+1.00	+0.71	+0.81	+1.00
	+0.18 ^c	+0.75 ^c			+0.78
		+0.58			+0.70
		+0.23			
$E_{\text{red}} (\text{V})$					
−0.74	−0.03	−0.03 ^b	−0.35	+0.33 ^c	+0.34 ^c
	−0.32 ^c	−0.40	−0.48	+0.09	+0.12 ^c
	−0.48 ^c	−0.75	−0.55	−0.09	+0.04 ^c
	−1.00 ^c		−0.71	−0.18	−0.08 ^c
	−1.24 ^c			−0.31 ^c	−0.19
				−0.39	−0.36
				−0.58 ^c	−0.53
					−0.68
					−1.15 ^c

^a All processes are one electron unless otherwise stated. ^b Two closely spaced one-electron processes. ^c Weak current signal presumably due to chemical product formation following a redox event.

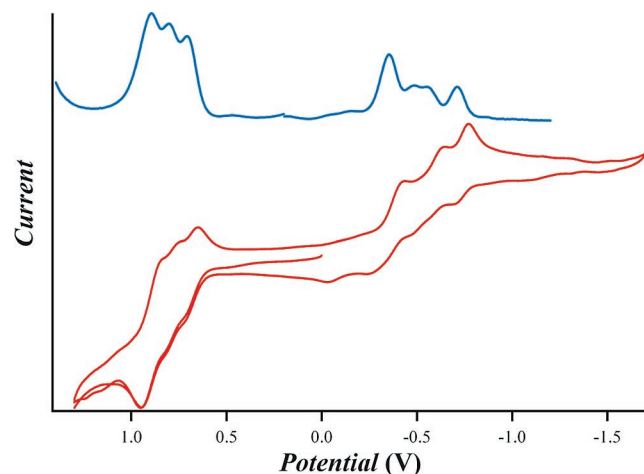


Figure 5. Electrochemical response (top: DPV, bottom: CV) of $[\{\text{CoCl}\}_4\{\text{Re}(\text{triphos})(\text{CN})_3\}]$ (**6**) recorded in 0.1 M $[\text{nBu}_4\text{N}][\text{PF}_6]/\text{CH}_3\text{CN}$. Potentials reported vs Ag/AgCl reference electrode.

4, and **6–8** indicate significant metal–metal coupling occurs in these clusters. Redox potentials for the compounds are listed in Table 4. The starting material for the study, compound **1**, exhibits redox processes assigned to the oxidation of Re(II) to Re(III) (+0.19 V), reduction to Re(I) (−0.74 V), and oxidation of the Re(III) product to Re(IV) (+1.12 V).⁵¹ Figure 5 depicts the cyclic voltammograms (CV) and differential pulse voltammograms (DPV) for **6**, which is representative of the behavior observed for complexes **2**, and **6–8**. The cyclic voltammogram for **6** shows two sets of waves that each contain multiple split waves centered around +0.80 and −0.53 V, which were determined by electrolysis to be quasi-reversible oxidation and quasi-reversible reduction processes, respectively. The splitting of these waves in both sets (up to 130 mV for the reduction and 90 mV for the oxidation waves) indicates multiple metal-based redox processes experiencing metal–metal electronic coupling. The DPV waves for **6** indicate a total of seven waves corresponding to three oxidation and four reduction processes. The four reduction processes ($E_{1/2} = -0.35, -0.48, -0.55, -0.71$ V) are reasonably assigned to formally Re(II)→Re(I) due

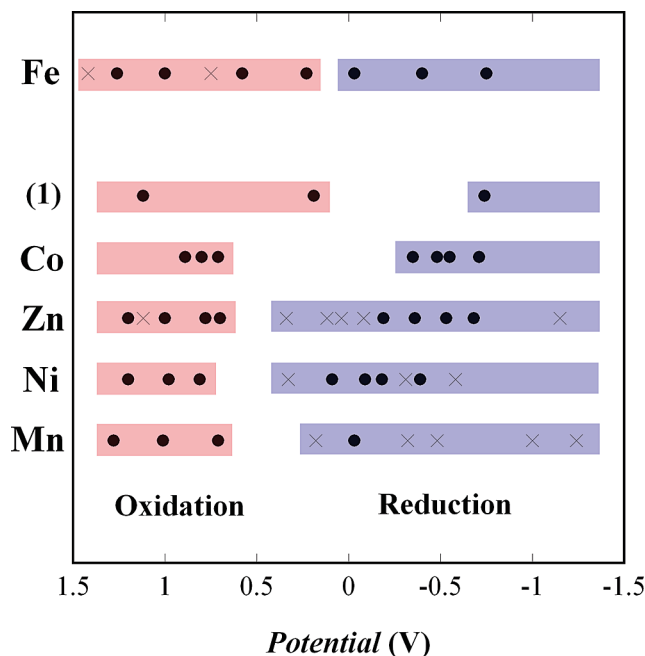


Figure 6. Summary of electrochemical processes (DPV) observed for **1–2**, **4**, and **6–8**. Solid points are assigned to primary cluster (or starting material) redox processes, whereas hollow points are assigned to products generated during subsequent chemical events.

to their similarity to the potentials for the reduction potentials of **1** (−0.74 V).

The three quasi-reversible oxidation processes observed for **6** (+0.89, +0.80, +0.71 V) occur at ~1.3 V higher potential than the reductions, which is comparable to the $\Delta E_{1/2}$ wave separation for the Re(II)→Re(I) and Re(II)→Re(III) processes in **1** (~1.0 V), noting that the Re(II)→Re(III) oxidation in the starting material is irreversible. More evidence for the assignment of the oxidation waves in this system as Re-based can be found by comparison of **6** with **8** (Figure 6). In the case of **8** the expectation is that Zn(II) ions will not be electrochemically active. In spite of the appearance of new electrochemical product waves, the same general trend is followed, namely one set each of oxidation and reduction processes, is observed. This indicates that the Re(II)→Re(III) electrochemistry is more accessible than the 3d metal ion redox processes in complexes **2** and **6–8**, although it is unclear why only three of the four possible oxidations are observed in **6**. In general, the oxidation and reduction potentials of the Re(II) ions in **2** and **6–8** occur at more positive potentials as a result of incorporation in the clusters. This change in potentials is most dramatic in the case of **2** and least in **6**.

The appearance of many new product waves in the electrochemistry of **2**, **7**, and especially **8** indicates that the clusters are undergoing chemical reactions, which likely involve fragmentation (Figure 6). This observation is consistent with the appearance of fragmentation products observed in the electrospray mass spectrum of **8**, presumably due to the lability of the Zn–L interactions. These processes are presumably also the reason that more cluster-based redox events are not observed in the case of **2**. The fragmentation of the clusters subsequent to oxidation is a reflection of a reorganization barrier for the reverse Re(III)→Re(II) process, manifest in the oxidation of **1** in the irreversibility of this process. In the clusters, the twelve nitrogen-bound metal–cyanide coordination bonds holding the

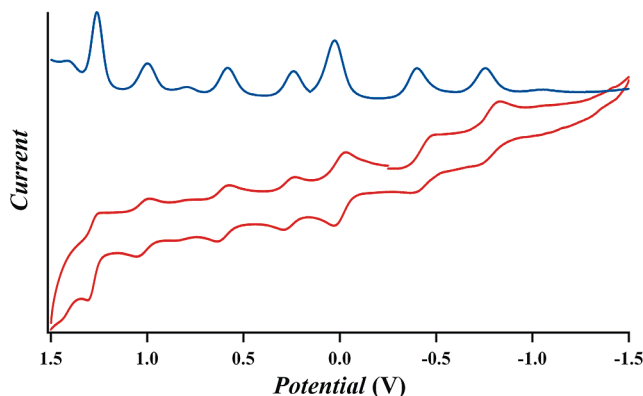


Figure 7. Electrochemical response (top: DPV, bottom: CV) of $[\{\text{FeCl}\}_4\{\text{Re}(\text{triphos})(\text{CN})_3\}_4]$ (**4**) recorded in 0.2 M $[\text{Bu}_4\text{N}][\text{PF}_6]/\text{CH}_3\text{CN}$. Potentials reported vs Ag/AgCl reference electrode.

molecules together presumably serve to exclude any accompanying chemical event to the $\text{Re}(\text{II}) \rightarrow \text{Re}(\text{III})$ oxidation, which lowers the reorganizational barrier for the reverse process. As such, the $\text{Re}(\text{II}) \rightarrow \text{Re}(\text{III})$ oxidation processes are observed in the clusters but with the development of additional positive charge eventually resulting in fragmentation.

The rhenium–iron cluster (**4**) exhibits a markedly different electrochemistry from the other members of the series (Figure 6). Figure 7 shows the CV and DPV waves for this complex which reveals the large number of quasi-reversible and reversible redox events that occur in this cluster. As discussed previously, upon formation, compound **4** exists in the formal oxidation states of $\text{Re}(\text{I})$ and $\text{Fe}(\text{III})$.³⁸ The four couples at +1.26, +1.00, +0.58, and +0.23 V are assigned as $\text{Re}(\text{I}) \rightarrow \text{Re}(\text{II})$ oxidation processes as judged by electrolysis experiments, while the three couples at −0.03, −0.40 and −0.75 V are assigned as $\text{Fe}(\text{III}) \rightarrow \text{Fe}(\text{II})$ reductions. Bulk electrolysis also revealed that the process at −0.03 V involves two electrons, presumably the result of two closely spaced one-electron process waves. The electrochemistry for this cluster is remarkable in that there is very little decomposition of the cluster throughout the potential range of the experiment, as judged by the relative current of the processes at +1.42 and +0.75 V. This is consistent with the electrospray mass spectrometry experiments that show only a single ion, unlike **2** and **6–8**, which reveal a degree of fragmentation. The reversibility of the $\text{Re}(\text{I}) \rightarrow \text{Re}(\text{II})$ oxidations for **4** is not supported by the reversibility of the same process in **1**. Additional oxidation processes for **4**, as observed for **2** and **6–8**, presumably lie at higher potentials outside of the electrochemical window of this experiment.

Magnetic Properties. General Considerations. Magnetic susceptibilities for **2**, **4** and **6** have been reported previously^{18,38} and are summarized below. The magnetic susceptibilities of compounds **3**, **5** (see Supporting Information), **7**, and **8** were recorded in the range of 1.8–300 K. As was noted previously for complexes **2**, **4**, and **6** the susceptibilities of **3**, **5**, **7**, and **8** are characterized by a strong temperature-independent $\text{Re}(\text{II})$ paramagnetic contribution and coupling between the $\text{Re}(\text{II})$ and 3d metal ions, which is manifested at low temperatures. The magnetic moment of the $\text{Re}(\text{II})$ ion is referred to as “ $S = 1/2$ ” for simplicity, with the understanding that the ion exhibits an orbital $2E$ magnetic ground state.^{35–37} Intercluster magnetic

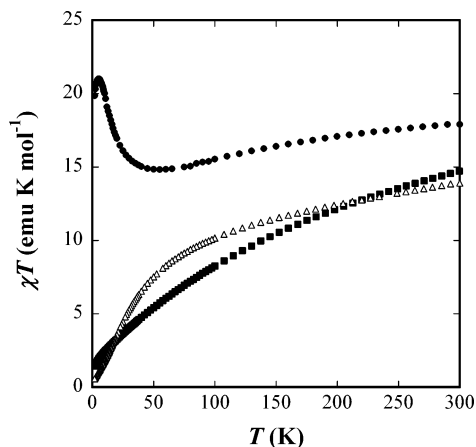


Figure 8. Temperature-dependent magnetic susceptibility data for $[\{\text{MnCl}\}_4\{\text{Re}(\text{triphos})(\text{CN})_3\}_4]$ (**2**), $[\{\text{FeCl}\}_4\{\text{Re}(\text{triphos})(\text{CN})_3\}_4]$ (**4**), and $[\{\text{CoCl}\}_4\{\text{Re}(\text{triphos})(\text{CN})_3\}_4]$ (**6**) recorded in the range of 1.8–300 K.

interactions are negligible, due to the large intercluster metal–metal separations ($> 10 \text{ \AA}$).

$[\{\text{MnCl}\}_4\{\text{Re}(\text{triphos})(\text{CN})_3\}_4]$ (**2**). Temperature-dependent magnetic susceptibility data for **2** are dominated by the signature of antiferromagnetic coupling between the “ $S = 1/2$ ” $\text{Re}(\text{II})$ and $S = 5/2$ $\text{Mn}(\text{II})$ ions (Figure 8).¹⁸ The room-temperature χT vs T value of $17.90 \text{ emu K mol}^{-1}$ is consistent with four isolated $\text{Re}(\text{II})$ ions and four isolated $\text{Mn}(\text{II})$ ions. Using the value established for the parent $\text{Re}(\text{II})$ complex **1** of $0.63 \text{ emu K mol}^{-1}$ at 300 K, a magnetic moment of $5.55 \mu_B$ per $\text{Mn}(\text{II})$ ion is obtained compared to the predicted value of $5.92 \mu_B$ when $g = 2$ for this ion. The value of the χT product decreases with temperature, indicating antiferromagnetic coupling of the $\text{Re}(\text{II})$ and $\text{Mn}(\text{II})$ ions, reaching a minimum at $\sim 55 \text{ K}$. This minimum is followed by an abrupt increase of the χT product, which attains a maximum value at 5 K. This behavior is consistent with incomplete cancellation of the $\text{Re}(\text{II})$ and $\text{Mn}(\text{II})$ “spins” and the attainment of an “ $S = 8$ ” ground state.

Due to the large spin ground state of the complex, its magnetization reversal dynamics were probed with the use of AC susceptometry. While low-frequency experiments illustrated frequency dependence, high oscillation frequencies were ultimately required to observe the peak in the out-of-phase component of the signal. The peak temperatures were fit to an Arrhenius relationship: $\Delta E = \tau_0 \exp(U_{\text{eff}}/k_b T)$, leading to an effective barrier height for magnetization reversal of $U_{\text{eff}} = 8.8 \text{ cm}^{-1}$ and a preexponential value $\tau_0 = 3.25 \times 10^{-7}$.¹⁸

To further explore the SMM behavior reported for **2**,¹⁸ hysteresis loops were collected on easy-axis oriented single-crystal samples using a micro-SQUID apparatus. Temperature-dependent scans reveal hysteretic behavior for **2** at low temperatures, with strongly temperature- and sweep rate-dependent coercivity. The coercivity increases with decreasing temperature and increasing field sweep rate. These data further confirm the SMM behavior of **2** (Figure 9 and Supporting Information).^{32,60} The data also reveal a prominent step at zero field which results from fast tunneling relaxation of the magnetization. The step becomes temperature independent below 0.2 K but remains sweep rate-dependent, consistent with a ground-state resonant tunneling process at $H = 0$.

(60) Hendrickson, D. N.; Yang, E.-C.; Isidro, R. M.; Kirman, C.; Lawrence, J.; Edwards, R. S.; Hill, S.; Yamaguchi, A.; Ishimoto, H.; Wernsdorfer, W.; Ramsey, C.; Dalal, N.; Olmstead, M. M. *Polyhedron* **2005**, *24*, 2280.

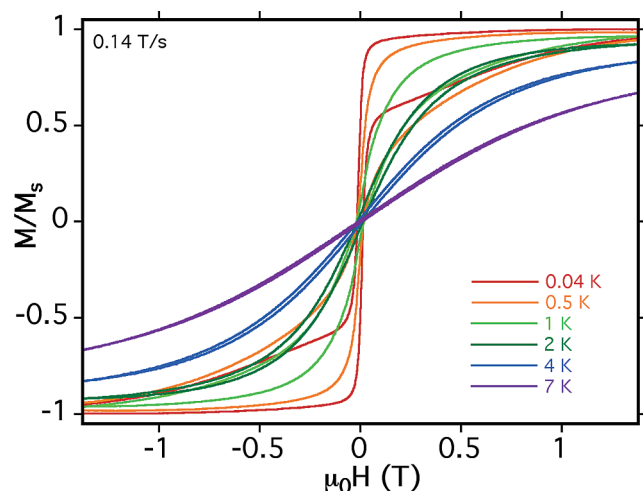


Figure 9. Temperature-dependent micro-SQUID magnetization scans collected for $[\{\text{MnCl}\}_4\{\text{Re}(\text{triphos})(\text{CN})_3\}_4]$ (**2**) at 0.14 T/s showing hysteretic behavior at 0.04 K and a fast tunneling relaxation process at $H = 0$. Magnetization values are normalized to the magnetization value at 1.4 T.

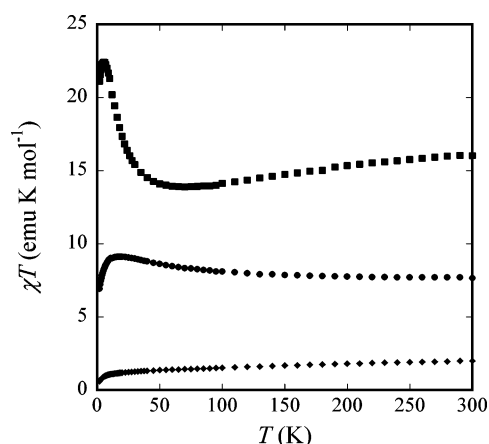


Figure 10. Temperature-dependent magnetic susceptibility data for $[\{\text{MnI}\}_4\{\text{Re}(\text{triphos})(\text{CN})_3\}_4]$ (**3**) (■), $[\{\text{NiCl}\}_4\{\text{Re}(\text{triphos})(\text{CN})_3\}_4]$ (**7**) (●), and $[\{\text{ZnCl}\}_4\{\text{Re}(\text{triphos})(\text{CN})_3\}_4]$ (**8**) (◆) recorded in the range of 1.8–300 K.

Several factors contribute to magnetization tunneling and destruction of the slow superparamagnetic relaxation in zero field for **2**: (i) the single-ion anisotropies of the magnetic center cancel each other, leading to a low effective anisotropy of the molecule (see the description of **8** below); (ii) although spin–orbit coupling is important to yield strong single-ion anisotropies, it often leads to strong transverse magnetic anisotropies. Unless the latter is not canceled by symmetry, it leads to mixing of the ground-state multiplets and enhances quantum tunneling. This effect is perhaps lessened compared to that for Co(II) clusters, but such relaxation pathways probably also exist for **2**; (iii) perhaps most importantly in this case, seemingly all metal–cyanide SMMs reported to date suffer from small J values (Table 1), which introduce accessible manifolds of S states that allow relaxation of magnetization.

$[\{\text{MnI}\}_4\{\text{Re}(\text{triphos})(\text{CN})_3\}_4]$ (3**).** The temperature-dependent magnetic behavior of compound **3** (Figure 10) exhibits similar features to that of **2**.¹⁸ The $\chi_m T$ value is 16.02 emu K mol^{−1} at 300 K, which corresponds to a value of 3.38 emu K mol^{−1} (5.20 μ_B) per Mn(II) ion, using the value of 0.63 emu K mol^{−1} obtained for the parent Re(II) complex.⁵¹ The high-

temperature moment of the complex is in accord with the expected value per Mn(II) ion (5.92 μ_B) for isolated magnetic ions. With decreasing temperatures, the $\chi_m T$ product decreases until ~ 70 K where it exhibits a broad minimum, which is followed by an abrupt increase in $\chi_m T$ to a value of 22.42 emu K mol^{−1} at 5.5 K. As in the case of **2**, this behavior is consistent with an antiferromagnetic interaction between the Re(II) and Mn(II) ions. AC susceptometry revealed a signal in χ'' with frequency dependence, indicating that **3** also behaves as a single molecule magnet, although the barrier height U_{eff} could not be determined using the experimental parameters of 1.8–5.0 K and 1–1000 Hz (see Supporting Information).

$[\{\text{FeCl}\}_4\{\text{Re}(\text{triphos})(\text{CN})_3\}_4]$ (4**).** As described above and previously,³⁸ electron transfer that occurs concomitant with formation of **4** yields a ground-state electronic configuration of Re(I)₄Fe(III)₄ for this cluster. The magnetic behavior of **4** results primarily from the $S = 5/2$ Fe(III) ions with a small temperature-independent paramagnetic contribution from the low-spin d⁶ Re(I) ions (Figure 8). The χT product at 300 K for **4** of 14.72 emu K mol^{−1} yields a value of 5.43 μ_B per Fe(III) ion, consistent with the predicted value of 5.92 μ_B . The χT vs T response for **4** decreases with temperature monotonically, reaching a value of 1.45 emu K mol^{−1}. The temperature-dependent behavior results from TIP and, presumably, next-nearest neighbor Fe(III)–Fe(III) antiferromagnetic interactions at low temperatures.

$[\{\text{CoCl}\}_4\{\text{Re}(\text{triphos})(\text{CN})_3\}_4]$ (6**).** Temperature-dependent susceptibility data for **6** are shown in Figure 8. At 300 K compound **6** exhibits a magnetic moment of 4.77 μ_B per ⁴A₂ Co(II) ion, a value consistent with data reported for tetrahedral Co(II) ions that possess an orbital angular momentum component from admixture of the ⁴T₂ excited state.⁶¹ The data are consistent with an antiferromagnetic interaction between the Co(II) and Re(II) ions through the decrease observed in $\chi_m T$ vs T . The small value (0.58 emu K mol^{−1}) observed in the $\chi_m T$ vs T plot for **6** at low temperature indicates the “spins” of the ions are canceling each other nearly completely. This is the result of a positive zero field splitting for the $S = 3/2$ Co(II) ions, resulting in a thermally populated effective spin $S = 1/2$ at low temperatures.⁶² As such, the true magnetic ground state for **6** exhibits no first-order Zeeman effect with the residual paramagnetism being due only to TIP.³⁸

$[\{\text{NiCl}\}_4\{\text{Re}(\text{triphos})(\text{CN})_3\}_4]$ (7**).** The magnetic properties of **7** are depicted in Figure 10. The $\chi_m T$ vs T data for **7** exhibit a value of 7.67 emu K mol^{−1} at 300 K, which, according to the convention established above, corresponds to 1.29 emu K mol^{−1} (3.21 μ_B) per Ni(II) ion. This value is in agreement with reported values for complexes of Ni(II) ions in a distorted tetrahedral coordination environment (3.0–3.5 μ_B , t^2 configuration),⁶¹ for which there is an first-order orbital angular momentum component to the magnetic moment. The value of $\chi_m T$ vs T increases gradually with decreasing temperature until it reaches a maximum of 9.12 emu K mol^{−1} (8.54 μ_B) at 18 K. Below 18 K $\chi_m T$ decreases rapidly, reaching a value of 6.93 emu K mol^{−1} (7.45 μ_B) at 2 K. The increase in $\chi_m T$ vs T values with decreasing temperature is an indication of ferromagnetic coupling between the metal ions in this complex, the only example in the series

(61) Cotton, F. A.; Wilkinson, G.; Bochmann, M.; Murillo, C. *Advanced Inorganic Chemistry*, 6th ed.; Wiley: New York, 1998.

(62) Carlin, R. L. *Magnetochemistry*; Springer-Verlag: Berlin, 1989.

to exhibit such coupling. For $g = 2$, the value at the low-temperature maximum in the $\chi_m T$ vs T plot of $9.12 \text{ emu K mol}^{-1}$ ($8.54 \mu_B$) at 18 K is lower than that expected for a $S = 6$ cluster ($21.00 \text{ emu K mol}^{-1}$) but higher than the value calculated for $S = 2$ ($3.00 \text{ emu K mol}^{-1}$) which would be the result of antiferromagnetic coupling. These data indicate that the cluster exhibits an overall g value < 2 . No signal was observed in χ'' of the AC susceptibility experiment for this cluster down to 1.8 K.

[{ZnCl}₄]{Re(triphos)(CN)₃}]₄ (8**).** The magnetic behavior of **8** is a function of only the Re(II) ions, as expected due to presence of diamagnetic Zn(II). The data reveal a monotonic decreasing $\chi_m T$ vs T response in the temperature range of 300–30 K, indicating the presence of strong temperature-independent paramagnetism (TIP) (Figure 10).^{35–37} The TIP for **8** is $2.39 \times 10^{-3} \text{ emu K mol}^{-1}$, based on a linear fit of the data ($R = 0.995$) between 100 and 300 K; however a curvature of the temperature dependence in the data over this range cannot be accounted for only by TIP. The high-temperature $\chi_m T$ vs T product is $2.00 \text{ emu K mol}^{-1}$, which is lower than the expected value of $2.52 \text{ emu K mol}^{-1}$ calculated from 4 times the value expected for the parent compound, **1**, at this temperature. The difference in the magnetic response of this compound as compared to the starting material arises from the overall geometry of the ions in the cluster. While these magnetic measurements were performed on averaged, powdered samples, the magnetic anisotropies of each uncoupled Re(II) ion are situated at the vertices of a tetrahedron such that the moments of the individual easy axes, which are predicted to lie along the C_3 axes,³⁶ are perturbed by the three others in the molecule. The effect that is observed in this case is a reduction in the isolated magnetic moments. Such anisotropy cancellation has been previously discussed,⁶³ and this structure allows for direct observation of the effect. The χ_{TIP} contribution is also affected by the geometry of the ions in the cluster, as it also exhibits a diminished response.

Below $\sim 30 \text{ K}$ $\chi_m T$ vs T decreases rapidly, reaching a value of $0.60 \text{ emu K mol}^{-1}$ at 2 K. This low-temperature value indicates antiferromagnetic coupling interactions are occurring between the Re(II) ions mediated by the NC–Zn(II)–CN linkages. Such next-nearest neighbor magnetic interactions have been noted for other metal–cyanide clusters.¹⁰ The possibility that **8** also has a component of geometric frustration to its magnetic response cannot be discounted, but the anisotropy of the Re(II) ions prevents thorough analysis in this context.

Conclusions

A family of metal–cyanide cubes has been prepared by a general synthetic procedure that demonstrates a powerful approach for the synthesis of a series of isostructural pseudo-cubic magnetic clusters. The redox activity of the Re(II) ion in these clusters affords a product with unexpected oxidation states

in the case of **4**, a cluster that exhibits a remarkable eight electron change in electronic configuration without decomposition of the cluster as determined by electrochemical studies. The compound is poised to be exploited for chemical redox studies aimed at isolating the various members of the series ranging from Re(II)₄Fe(III)₄ to Re(I)₄Fe(II)₄. It is also an attractive candidate for photomagnetic studies.⁶⁴ A rich solution electrochemistry of the other members of the series was also observed, the results of which showed both intact clusters as well as fragmentation. Within the series, all compounds exhibit antiferromagnetic coupling through the cyanide bridge except for **7**, which is ferromagnetically coupled. Despite the large low-temperature magnetic moment observed for compound **8**, only compounds **2** and **3** exhibit slow paramagnetic relaxation, which was further confirmed by micro-SQUID magnetization experiments performed on **2**. The results indicate that the molecule exhibits fast tunneling rates at zero field and strong sweep rate dependence. The fast tunneling relaxation process observed for **2** presumably arises from relaxation pathways via low-lying excited states due to weak magnetic coupling in the cluster.

The replacement of MnI₂ for MnCl₂ in the synthesis of compound **3** is a sufficiently small perturbation on the system such that the temperature-dependent susceptibility and SMM behavior observed for **3** is quite similar to that observed for **2**. The presence of iodide rather than chloride in these clusters is convenient in that it will be more easily displaced in substitution reactions.⁶⁵ The observation of a disordered component in the structure of **5** containing a partially occupied molecule of tetrahydrofuran coordinated to the Fe(I) site offers evidence for the feasibility of substitution reactions at the 3d metal ion sites. Finally, it is noted that appropriate chemical modification of the clusters with suitable linker groups would provide a rational synthetic approach to linking SMMs through coordination bonds.⁶⁶

Acknowledgment. K.R.D gratefully acknowledges the Department of Energy (DE-FG03-02ER45999), National Science Foundation (NIRT-NSF DMR-0103455), the Welch Foundation A1449, and Texas A&M University for funding of this research. The SMART CCD diffractometer and the SQUID magnetometer were purchased by funds provided by the National Science Foundation (Grants NSF-9807975 and NSF-9974899). Use of the TAMU/LBMS Applications Laboratory, Ms. Vanessa Santiago, and Dr. Shane E. Tichy are acknowledged. John Bacsa is acknowledged for a preliminary contribution.

Supporting Information Available: Synthetic details for **2–8**; magnetic data for **2, 3, 5, 7**, and **8**; molecular structures and tables of structural parameters for **7** and **8**. X-ray crystallographic data as CIF. This material is available free of charge via the Internet at <http://pubs.acs.org>.

JA0683281

(63) Bonadio, F.; Gross, M.; Stoeckli-Evans, H.; Decurtins, S. *Inorg. Chem.* **2002**, *41*, 5891.

(64) Herrera, J. M.; Marvaud, V.; Verdaguer, M.; Marrot, J.; Kalisz, M.; Mathoniere, C. *Angew. Chem., Int. Ed.* **2004**, *43*, 5468.

(65) Berlinguette, C. P.; Dunbar, K. R. *Chem. Commun.* **2005**, 2451.

(66) Hill, S.; Edwards, R. S.; Aliaga-Alcalde, N.; Christou, G. *Science* **2003**, *302*, 1015.